 MCB, vol.11, no.2, pp.129-149, 2014

Fluid-Structure Interaction Analysis of Pulsatile Flow within a Layered and Stenotic Aorta

Zheng-qi Liu[*], Ying Liu[*,†], Tian-tian Liu[*] and Qing-shan Yang[‡]

Abstract: In this paper, the hemodynamic characteristics of blood flow and stress distribution in a layered and stenotic aorta are investigated. By introducing symmetrical and unsymmetrical stenosis, the influence of stenosis morphology and stenotic ratio on the coupled dynamic responses of aorta is clarified. In the analysis, the in-vivo pulsatile waveforms and fully fluid–structure interaction (FSI) between the layered elastic aorta and the blood are considered. The results show that the fluid domain is abnormal in the stenotic aorta, and the whirlpool forms at the obstructed and downstream unobstructed regions. The maximum wall shear stresses appear at the throat of the stenosis. Downstream region appears low and oscillated shear stresses. In addition, along with the increase of the stenotic ratio, the amplitude of the maximum shear stress will be intensively increased and localized, and the sensitivity is also increased. In the aorta with unsymmetrical stenosis, the Von Mises stresses reach the peak value at the side with the surface protuberance, but they are reduced at the side with no protuberance. The sign variation of the layer interface shear stresses near the throat indicates the variation of the shear direction which increases the opportunity of shear damage at the transition plane. Moreover, the shear stress levels at the fluid-solid and intima-media interfaces are higher than that at the media-adventitia interface. The unsymmetrical stenosis causes higher stresses at the side with the surface protuberance than symmetrical one, but lower at the side with no protuberance. These results provide an insight in the influence of the stenosis, as well as its morphology, on the pathogenesis and pathological evolution of some diseases, such as arteriosclerosis and aortic dissection.

Keywords: Aorta, Stenosis, Fluid-structure interaction, Hemodynamic characteristic, Stress distribution.

[*] Department of Mechanics, School of Civil Engineering, Beijing Jiaotong University, Beijing, 100044, P.R. China.

[†] E-mail: yliu5@bjtu.edu.cn; Tel: 86-10-51682094; Fax: 86-10-51682094.

[‡] School of Civil Engineering, Beijing Jiaotong University, Beijing, 100044, P.R. China.

1 Introduction

As the race of life in the modern world grows more and more fast, and the social pressures are increased, the incidence of cardiovascular disease bursts out. Cardiovascular disease has become one of the most dangerous diseases and displays worrying expectation since it becomes diseases incidental to young people. World Health Organization (WTO) has listed it as one of the three diseases which are most harmful to human health due to its high mortality. Consequently, understanding the pathogenesis and pathological evolution of these diseases, such as arteriosclerosis and aortic dissection, has significant meaning for disease prevention and treatment.

Clinical research shows that hemodynamic characteristics of arterial blood flow, as well as the arterial lesion, play important roles in the origination and evolution of cardiovascular disease. A lot of researches have been carried out to investigate the hemodynamic properties of arterials. However, it is more and more realized that except for the physiological performance, the mechanical environment of arteries also plays an important role in the generation of vascular diseases, especially when the arterial lesion exists. Detailed knowledge about the mechanical behavior of arteries with lesion is essential for the improvement of (non-) surgical procedures and the development of prosthetic materials and tissue equivalents.

Gao *et al*. [1] conducted a numerical study to analyze the stress distribution in a three-layered aorta under pulsatile flow by applying an unreal zero pressure condition at aortic outlet. Khanafer and Berguer [2] discussed the radial stress distribution based on the perfect three-layered elastic aorta model by using the true physiological inlet velocity and outlet pressure. In their work, the aortic lesion is not considered. Ang and Mazumdar [3] investigated the influence of the unsymmetrical stenosis on the arterial wall stress using a rigid vessel wall model. Kagadis *et al*. [4] developed a severe stenotic renal artery model for the description of the hemodynamic characteristics and stress distribution in the artery. But owing to the rigid wall assumption, the coupling effects between the vessel wall and the blood flow were not considered. Recently, Bark and Ku [5] quantified the largest wall shear rates that might occur in a diseased coronary artery during the cardiac cycle, and defined the hemodynamic conditions for occlusive thrombosis. However, the physiological structure of the artery was ignored in their work. Melih Guleren [6] analyzed the flow characteristics through specific concentric and eccentric plaque formations, but the stress distribution in the arterial wall was not investigated. Obviously, although the hemodynamic characteristics of blood flow in artery have been widely investigated, the coupled responses between the layered artery and the blood, as well as the stenosis morphology and stenotic ratio, still needs more detailed investigation.

Anatomy demonstrates that the artery is layer-structured [7]. Different layers have different material properties and thicknesses. Moreover, due to the complexity of pathological evolution process, stenosis morphology is always non-symmetrical. Near the stenosis, the blood flowing property changes which in turn affects the stress distribution in the artery. Aiming to provide a mechanical understanding of the roles played by the stenosis on the pathogenesis and pathological evolution of aortic disease, a FSI analysis is carried out based on a three-layered aorta model. By introducing the in-vivo pulsatile waveforms, the influence of the localized stenosis on the blood flow and the stress distribution in the aorta is discussed in detail. At last, the conclusion is given.

2 Calculating model

2.1 Aorta Model

Physiologically, an aorta is approximately a three-layered heterogeneous structured composite vessel. In our present calculation, according to Khanafer and Berguer [2], the inner diameter of the aorta is set to be 24mm. The thickness of the whole wall is chosen to be 2mm, and the thicknesses of the intima, media, and adventitia are taken as 0.2, 1.2 and 0.6mm respectively. In order to manifest the intrinsic influence of stenosis on the stress distribution in the vessel wall, the geometrical and physical nonlinearity of the vessel is not considered here. Each layer is isotropic with elastic modulus 2, 6, and 4MPa, respectively. The Poisson's ratio is υ=0.45, and the density ρ_s=1100kg/m^3. Likewise, the density of the blood in the aorta is ρ_f=1050kg/m^3, and the viscosity μ=0.00345Pa·s.

Following Forrester and Young [8], the original virtual symmetrical stenotic aorta model is functioned as

$$R = \mathrm{R}_0 - \frac{h}{2}\left(1 + \cos\frac{\pi z}{\mathrm{Z}_0}\right) \qquad -\mathrm{Z}_0 \le z \le \mathrm{Z}_0, \tag{1}$$

where R is the aorta inner radius at the stenosis, h is the stenosis height, Z_0 is the half length of the stenosis and we define $Z_0 = R_0$, the inner radius of the unobstructed part of the aorta.

Correspondingly, the unsymmetrical stenotic aorta model is described as

$$D = \mathrm{D}_0 - \frac{h}{2}\left(1 + \cos\frac{\pi z}{\mathrm{Z}_0}\right) \qquad -\mathrm{Z}_0 \le z \le \mathrm{Z}_0\,, \tag{2}$$

where D is the inner diameter at the stenosis, D_0 is the inner diameter of the unobstructed part of the aorta.

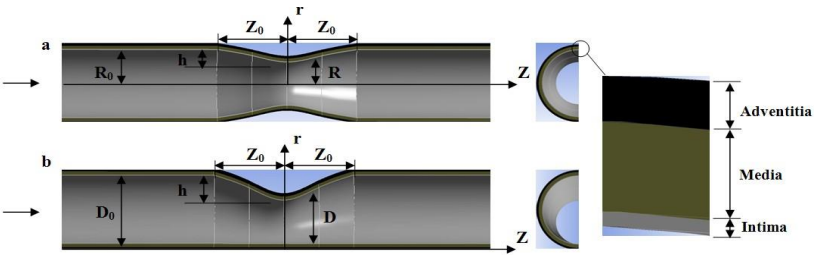

Figure 1: Diagrammatic sketch of stenotic aorta: a) symmetrical stenosis; b) unsymmetrical stenosis.

In order to facilitate the analysis, as shown in Fig.2, the model is divided into four regions from inlet to the outlet, that is, upstream unobstructed region (R1), upstream obstructed region (R2), downstream obstructed region (R3) and downstream unobstructed region (R4). Consequently, four critical planes are also defined, that is, S1, the middle cross section of R1; S2, the throat of the stenosis; S3, the interface section of R3 and R4, and S4, the middle cross section of R4.

The aorta length is L=168mm. We define stenotic ratio as

$$\delta = 1 - \frac{A}{A_0}, \tag{3}$$

where A is the lumen cross-sectional area of throat, A_0 is the lumen cross-sectional area of unobstructed part. In the present discussion, four stenotic ratios, that is, 0, 40%, 60%, and 80%, are considered.

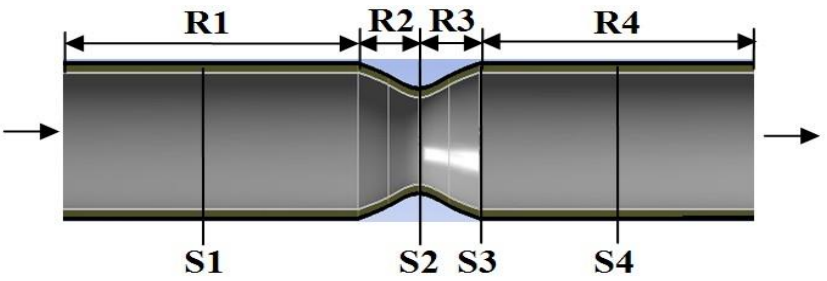

Figure 2: Diagrammatic sketch of the section partition and positions of critical planes.

2.2 Boundary conditions

In order to reflect the real physiological condition, a physiological velocity waveform is applied at the inlet and a physiological pressure waveform at the outlet [9]. As shown in Fig.3, inlet peak systolic flow occurs at t=0.4s, and exit peak systolic pressure at t=0.5s. The maximum Reynolds number is defined as $\mathrm{Re}_{max}=\rho_f u_{max} D_0/\mu=3218$ where u_{max} is the maximum fluid velocity.

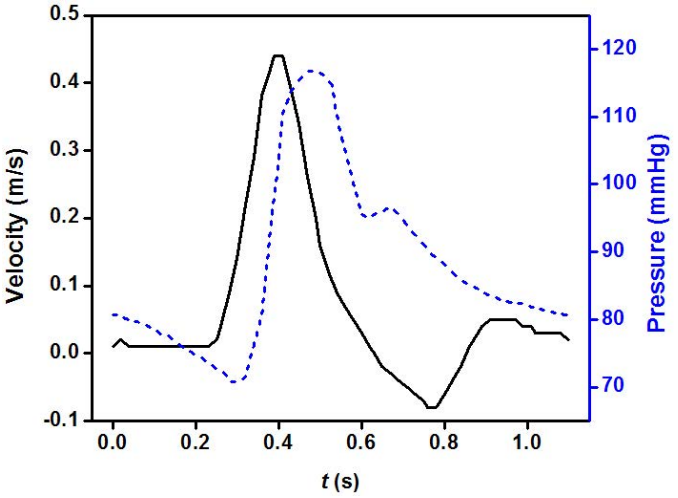

Figure 3: In-vivo recorded waveforms of pulsatile inlet mean velocity and outlet pressure.

Here k-ω model [10] is used to simulate the blood flow in the aorta since blood flow is not fully laminar or turbulent in a cycle, and k-ω model is adept in simulating the situation from the laminar flow to the turbulent flow. The transport equations for turbulent kinetic energy (κ) and turbulence frequency (ω) in the Wilcox model are

$$\frac{\partial}{\partial t}(\rho_f \kappa)+\frac{\partial}{\partial x_j}(\rho_f u_j \kappa)=\tau_{ij}\frac{\partial u_i}{\partial x_j}-\beta^*\rho_f\omega\kappa+\frac{\partial}{\partial x_j}\left[(\nu+\sigma^*\mu_T)\frac{\partial \kappa}{\partial x_j}\right], \tag{4}$$

$$\frac{\partial}{\partial t}(\rho_f \omega)+\frac{\partial}{\partial x_j}(\rho_f u_j \omega)=\alpha\frac{\omega}{\kappa}\tau_{ij}\frac{\partial u_i}{\partial x_j}-\beta\rho_f\omega^2+\frac{\partial}{\partial x_j}\left[(\nu+\sigma\mu_T)\frac{\partial \omega}{\partial x_j}\right], \tag{5}$$

where $S_{ij}=\frac{1}{2}\left(\frac{\partial u_i}{\partial x_j}+\frac{\partial u_j}{\partial x_i}\right)$, the eddy viscosity $\mu_T=\alpha^*\rho_f\kappa/\omega$, and the Reynolds stress tensor $\tau_{ij}=2\mu_T\left(S_{ij}-\frac{1}{3}\frac{\partial u_k}{\partial x_k}\delta_{ij}\right)-\frac{2}{3}\rho_f\kappa\delta_{ij}$. In the equations, t is time, x_i is the component of the position vector, u_i is the fluid velocity, p is the fluid pressure,

ν is the molecular viscosity, δ_{ij} is the Kronecker delta. The six parameters α^*, α, β^*, β, σ^*, and σ are closure coefficients whose values are given as

$$\alpha^* = \frac{\alpha_0^* + \mathrm{Re_T}/R_k}{1+\mathrm{Re_T}/R_k}, \quad \alpha = \frac{5}{9}\cdot\frac{\alpha_0+\mathrm{Re_T}/R_\omega}{1+\mathrm{Re_T}/R_\omega}\cdot(\alpha^*)^{-1}, \quad \sigma^* = \sigma = 1/2,$$

$$\beta^* = \frac{9}{100}\cdot\frac{5/18+\left(\mathrm{Re_T}/R_\beta\right)^4}{1+\left(\mathrm{Re_T}/R_\beta\right)^4}, \quad \beta = \frac{3}{40}, \alpha_0^* = \beta/3, \quad \alpha_0 = 1/10,$$

$R_\beta = 8$, $R_k = 6$, $R_\omega = 2.7$, with Re_T the turbulence Reynolds number defined as $\mathrm{Re_T} = \rho_f \kappa / \omega\nu$.

2.3 Numerical scheme

A combined finite element and finite volume method is employed to solve the governing equations of fluid-structure interaction model of aorta by using ANSYS/Workbench subject to the boundary conditions described above.

To test and assess mesh size of fluid domain, the number of elements is gradually increased. The optimum mesh size is determined when further decreasement in mesh size do not significantly change the shear stress any more. Therefore, Solid186, a high order 20 nodes element, is chosen in aortic wall discretization. Multizone sweeping meshing is used in the fluid domain, that is, hexagonal grid (three layers in the present calculation) is used at the interface, whilst tetrahedron in the inner domain. For symmetrical stenosis, when δ=40%, there are 9816 and 24677 elements for solid (Fig. 4a) and fluid (Fig. 4b) domains, respectively.

Based on the convergence analysis, a time step size of 2×10^{-2}s is used and periodic convergence solution is achieved after 2 cycles.

2.4 Model validation

In order to verify the accuracy of our model, by adopting the parameters used in Khanafer and Berguer [2], the Von Mises stress distribution along the aorta radial direction when δ=0 (normal aorta) is calculated and given in Fig. 5, in which Von Mises stress is defined as a function of the principal stresses σ_1, σ_2, and σ_3, as follows:

$$\sigma = \sqrt{\frac{(\sigma_1-\sigma_2)^2+(\sigma_1-\sigma_3)^2+(\sigma_2-\sigma_3)^2}{2}}. \tag{6}$$

It is seen that the results obtained by our model and the model of Khanafer and Berguer [2] coincide well with each other which verifies the accuracy of our calculation.

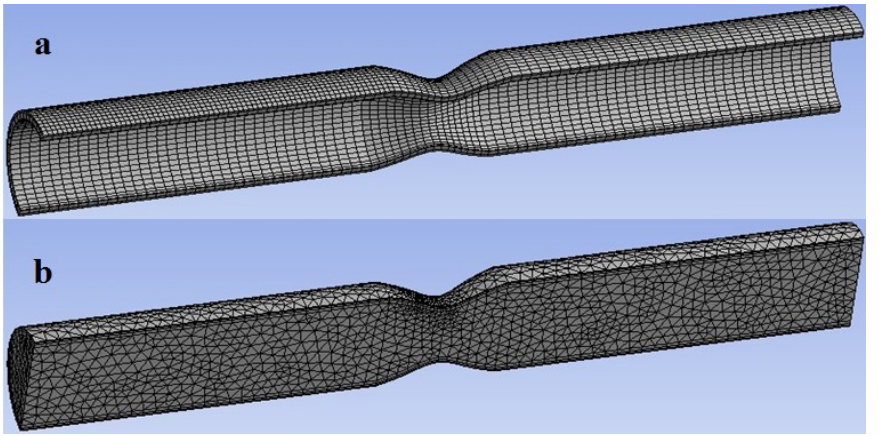

Figure 4: (a) Mesh of the solid domain; (b) mesh of the fluid domain.

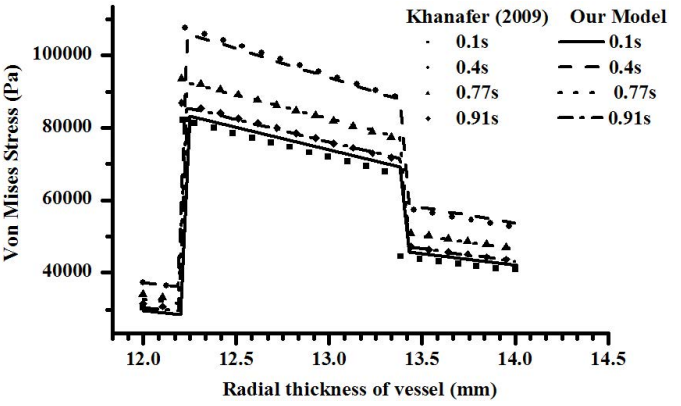

Figure 5: Variation of the Von Mises Stress along the radial direction in the aorta.

In order to verify the availability of k–ω model in the fluid domain calculation, referring to Priymak and Miyazaki [11], the fluid normalized axial velocity distribution in the pipe for Re=4000 is given in Fig. 6. Comparison with previous numerical [11] and experimental results [12] indicates that our model can well predict the fluid flow in the pipe.

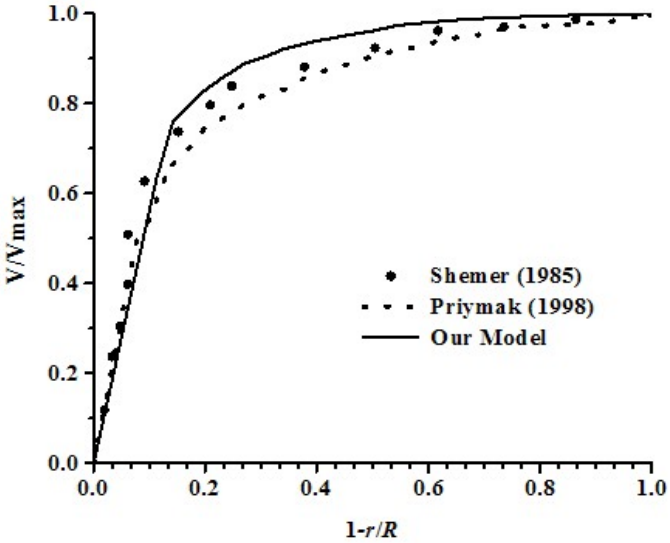

Figure 6: The normalized axial velocity in a pipe.

3 Numerical results and discussion

3.1 Fluid domain

According to Bernoulli equation, since the pressure and kinetic energy remain unchanged in a short distance, the variation of the diameter due to the stenosis must affect the hemodynamic characteristics greatly.

In order to illustrate this influence, the velocity and pressure contours within the normal aorta and aortas with symmetrical or unsymmetrical stenosis are given in Fig. 7. Four typical times, that is, t=0.1s (beginning of the systole), t=0.4s (peak systole), t=0.77s (end of systole), and t=0.91s (peak diastole), are chosen. When δ=0 (normal aorta, Fig. 7I), during 0.1s to 0.4s, ventricular and arterial pressures are both sharply increased. The flow is stable and the velocity reaches the peak value instantaneously. During 0.4s to 0.77s, the ventricular pressure is reduced; likewise, the flow velocity is decreased and reversed. During 0.77s to 1.1s, there

exists positive flow in the aorta. For aorta with stenosis, seen as Fig. 7II and 7III (δ=40%), during the whole time, the fluid pressure is reduced with increased fluid velocity at the throat because of the aortic diameter reduction; likewise, the fluid pressure is increased with reduced fluid velocity at R3 because of the regain of the aortic diameter. During 0.4s to 0.77s, due to the decreased and reversed flow, whirlpool is appeared in R3 and R4. During 0.77s to 1.1s, there is a positive flow in the aorta, and the area of whirlpool in R4 is expanded. It is noticed that stenosis morphology will affect the pressure and velocity distribution in the aorta. Comparison between Fig. 7II and 7III shows that for the unsymmetrical stenosis, the variations of the fluid velocity and pressures are more obvious and the values are bigger at the side with surface protuberance (Fig. 7 III). Moreover, the affecting domain of the whirlpool in the unsymmetrical model is expanded and becomes unsymmetrical.

The axial velocities at different cross sections are given in Fig. 8. The corresponding values in the normal aorta are also plotted for comparison. The horizontal coordinate values represent that the distance from one side of aorta to the other side divided by the inner diameter. For the unsymmetrical stenosis, the distance is defined as that from the side with no protuberance to the side with the surface protuberance. When δ=0 (normal aorta), it is seen that the velocities at different cross sections are basically the same. During 0.1s to 0.4s, the velocities reach the peak values instantaneously. During 0.4s to 0.77s, the velocities are decreased and reversed. During 0.77s to 1.1s, the blood flow is positive. When δ=40%, the axial velocities at S1 change little which indicates that the stenosis has no significant effect on this section. For the symmetrical stenosis, the velocities at S2 increase significantly near the aortic wall (at t=0.77s, the flow is reversed). This is due to the reduction of the aortic diameter at S2. At S3, the aortic diameter recovers to the normal one which leads to the appearance of adverse pressure gradient, and the flow reverses partly. Consequently, there have both positive and negative blood flow at t=0.4s and t=0.77s at S3. Positive and negative blood flow also exist simultaneously at t=0.77s at S4 with the appearance of whirlpool. It is noticed that when the stenosis becomes unsymmetrical, the variation rules of the axial velocities at different sections are similar, expect that the distribution of the velocities is unsymmetrical. At S2 and S3, the velocity variation becomes more severe, especially at the side with the surface protuberance. That is, at the same stenotic ratio, the unsymmetrical distribution of stenosis will increase the non-homogeneous distribution of velocities in the aorta, especially at the S2 and S3 sections.

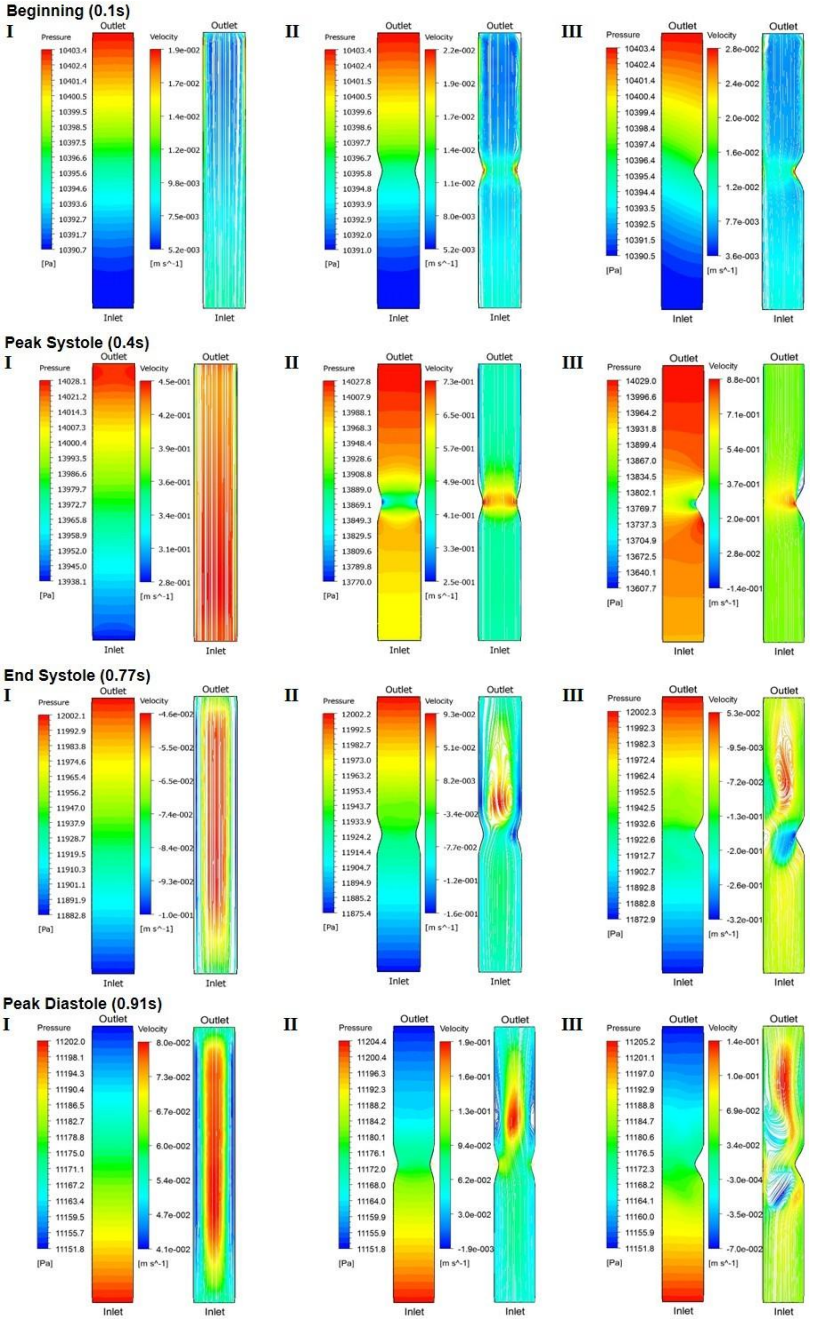

Figure 7: Pressure and velocity contours at different times in a cardiac cycle: I) δ=0; II) δ=40%, symmetrical stenosis; III) δ=40%, unsymmetrical stenosis.

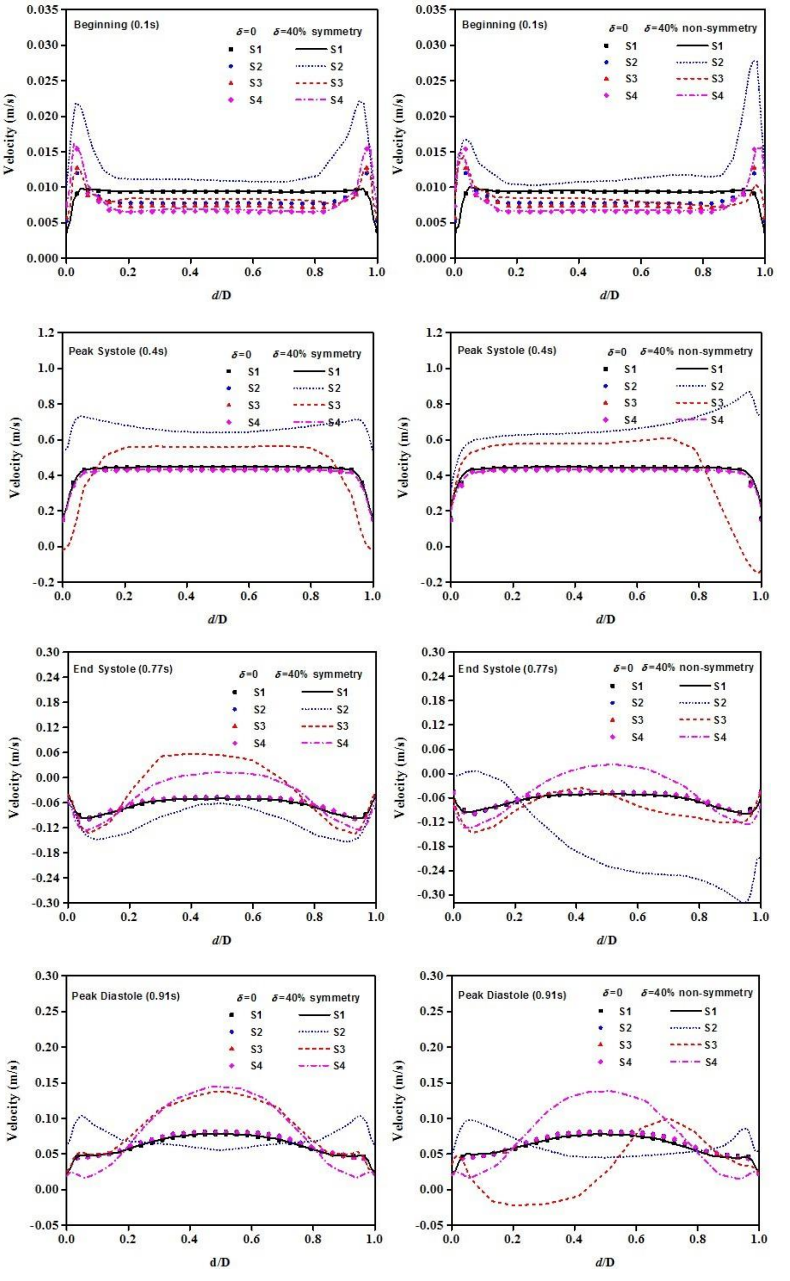

Figure 8: The axial velocities of different cross sections at different times in a cardiac cycle.

3.2 Turbulent kinetic energy and turbulent frequency

Figure 9 shows the variation of the turbulent kinetic energy κ and turbulent frequency ω at typical times. The turbulent kinetic energy is the kinetic energy per unit mass of the turbulent fluctuations in a turbulent flow. It is defined as

$$\kappa = \frac{1}{2}\left(\overline{u'_x{}^2} + \overline{u'_y{}^2} + \overline{u'_z{}^2}\right), \tag{7}$$

where u'_x, u'_y, u'_z are the turbulent average velocities along the direction x, y, and z, respectively.

When δ=0 (normal aorta, Fig. 9I), at t=0.1s, the flow velocity is low, so that the turbulent kinetic energy maintains low values in most regions except for the outlet due to the high outlet pressure. At t=0.4s, the inlet velocity reaches the peak value instantaneously which results in the maximum energy at inlet. At t=0.77s and 0.91s, the energy is confined in R1. When the stenosis forms (δ=40%, Figs. 9II and 9III), the energy distribution in R2 to R4 is changed because of the variation of the aortic diameter. At t=0.77s and 0.91s, the energy in domains R3 and R4 changes obviously, and whirlpool appears in R3 and R4. When the stenosis is unsymmetrical distributed (Fig. 9III), the position of the maximum κ is changed near to S1, and unsymmetrical (Fig. 9 III).

Analysis shows that the kinematic viscosity γ and the turbulent dissipation rate ε of the blood will affect the physiological environments in the aorta. Smallest turbulent eddies (Kolmogorov microscale), a function of γ and ε, is defined as

$$\eta = \left(\frac{\gamma^3}{\varepsilon}\right)^{0.25}, \tag{8}$$

where γ=μg/ρg. Liu *et al.* [13] found that if the Kolmogorov scale turbulent eddies were smaller than or similar in size to the blood cells, they would damage the cell membranes; otherwise when the turbulent eddies are much larger than the diameter of the blood cell, the eddies will not cause much damage.

Here the Kolmogorov microscales at the cross sections S1, S2, and S3 at the peak systole (t=0.4s) are calculated with the aim to investigate the effect of stenosis, as well as the stenosis morphology, on the cell membranes. For the unsymmetrical stenotic aorta model, we define the side with the surface protuberance as 'SPA' and the side with no protuberance as 'SPB'.

Table 1 illustrates the normalized Kolmogorov microscales $\bar{\eta}_\delta$ at different cross sections with $\bar{\eta}_\delta = \eta_\delta/\eta_{\delta=0}$. Absolutely, the smaller the values are, the greater the possible damage is. It is seen that at S1, $\bar{\eta}_\delta$ is less affected by the variation of the stenotic ratio. At S2 and S3, along with the increase of the stenotic ratio,

$\bar{\eta}_\delta$ is greatly decreased, which indicates the increased possibility of cell membrane damage near S2 and S3. For the unsymmetrical stenosis, the cell membrane damage at S2 on the SPA side is greatly increased since the absolute value and the variation ratio of $\bar{\eta}_\delta$ are both greatly decreased. That is, for the unsymmetrical stenosis, the stenosis throat is most dangerous cross section due to the serious shrink of the aorta diameter.

Table 1: The values of the normalized Kolmogorov microscales when δ=40%, δ=60% and δ=80%, respectively.

		S1			**S2**			**S3**		
		$\bar{\eta}_{0.4}$	$\bar{\eta}_{0.6}$	$\bar{\eta}_{0.8}$	$\bar{\eta}_{0.4}$	$\bar{\eta}_{0.6}$	$\bar{\eta}_{0.8}$	$\bar{\eta}_{0.4}$	$\bar{\eta}_{0.6}$	$\bar{\eta}_{0.8}$
Symmetry		1.06	1.03	1.02	0.87	0.62	0.35	0.68	0.53	0.32
Non-symmetry	**SPA**	1.01	1.02	1.05	0.68	0.49	0.32	0.71	0.51	0.28
	SPB	0.99	0.97	0.92	0.84	0.65	0.47	0.72	0.41	0.24

3.3 Wall shear stresses

The research of Malek *et al*. [14] indicates that low and alternating wall shear stresses (WSS) have correlated with the incidence of atherosclerosis. Therefore, it is necessary to clarify the effects of stenosis and its morphology on the wall shear stresses. Fig. 10 shows the WSS along the axial direction at typical times when δ=0 and δ=40%. Seen as Fig.10, when δ=0 (normal aorta), the WSS increases gradually from the inlet to the outlet at t=0.1s. At the other times, the WSS remains almost unchanged. For the symmetrical stenosis, at t=0.1s, the WSS increases gradually from the inlet to the outlet and a sharp increase forms at the stenosis throat. At t=0.4s, maximum WSS is reached just before the throat of the stenosis (at Z=84mm), then the stress values are decreased and negative WSS region appears which indicates the generation of flow separation and recirculation regions. At t=0.77s, diastolic phase begins, the reverse blood flow lead to maximum WSS appears at the downstream of the throat and the whole WSS is negative. At t=0.91s, alternating negative low WSS appears in the R4. When the stenosis is unsymmetrical, the WSS at SPA side changes dramatically. It is seen that the WSS decreases close to 0 in the R2, but the maximum value at the throat is higher and the alternating WSS region is extended. For the WSS at SPB side, it reaches the maximum value near the throat at t=0.1s, t=0.4s and t=0.91s. Because of the reverse flow, the whole WSS is negative and it closes to 0 at the throat at$t$=0.77s. Moreover, we can observe that alternating low WSS appears in the R4 during the whole process.

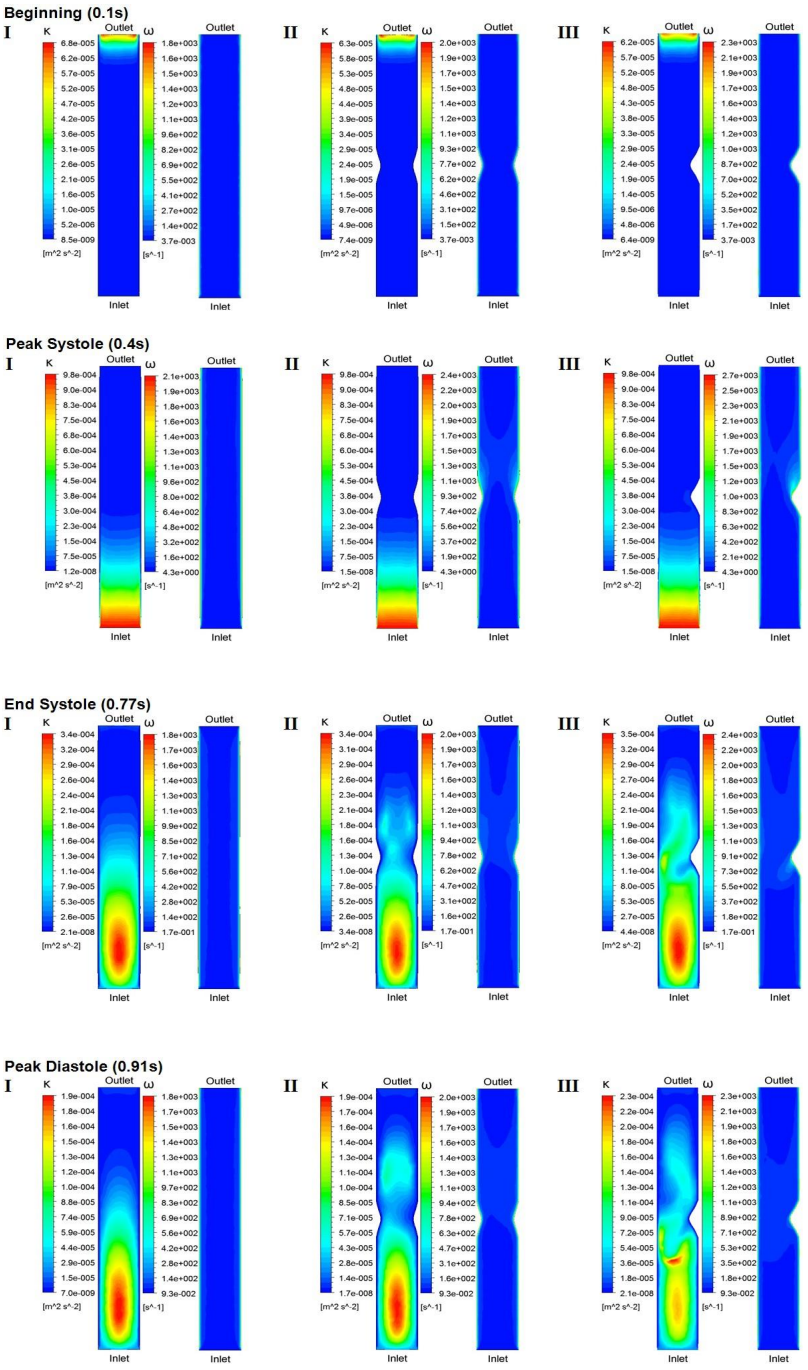

Figure 9: Turbulence kinetic energy (κ) and turbulence frequency (ω) in a cardiac cycle: I) δ=0; II) δ=40%, symmetrical stenosis; III) δ=40%, unsymmetrical stenosis.

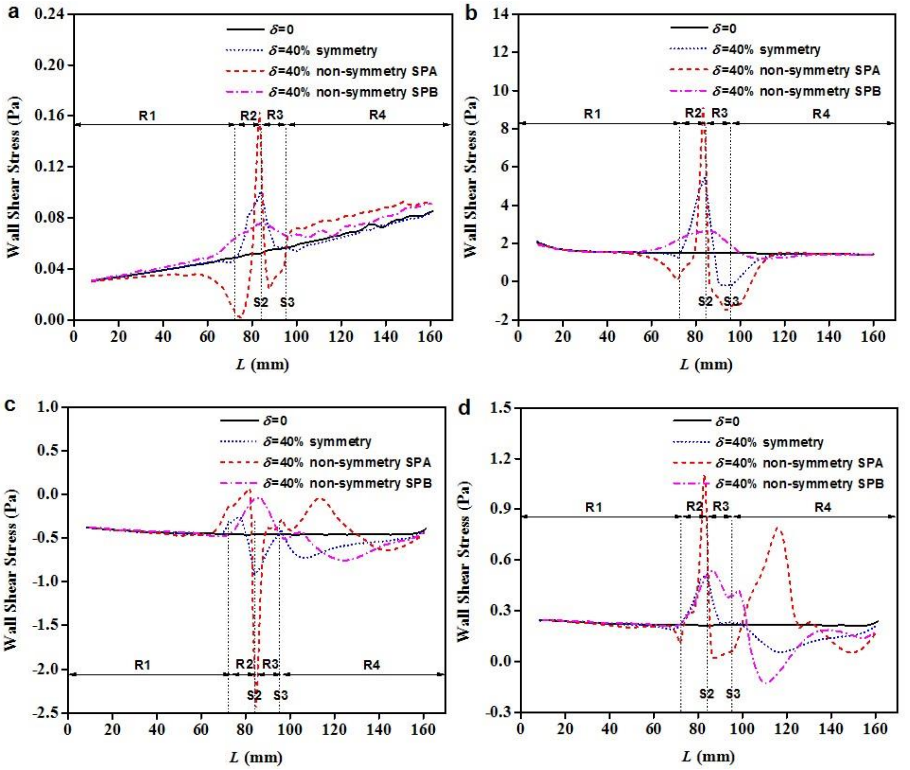

Figure 10: Variation of wall shear stress along the axial direction: a) t=0.1s; b) t=0.4s; c) t=0.77s; d) t=0.91s.

The above results show that the maximum WSS is reached just before the throat of the stenosis (upstream surface) at peak systole, and alternating low WSS appears in the downstream unobstructed region. Alternated positive and negative WSS indicates the existence of flow separation and recirculation region. Compared with symmetrical model, WSS at SPA side of unsymmetrical stenosis is reduced in the R2 and R3, and even closes to 0; whilst the maximum value is about twice of that for symmetrical stenosis. Moreover, flow separation and recirculation is more obvious. This result is consistent with that of Ang and Mazumdar [3].

In order to see the effects of stenotic ratio on the WSS, Fig.11 shows the variation of WSS at t=0.4s with respect to the stenotic ratio. The results for normal aorta (δ=0) are also given for comparison. Seen as Fig. 11a, for aorta with symmetrical stenosis, in R1, WSS is not sensitive to the variation of δ. The maximum WSS is reached just before the throat of the stenosis, and alternating low WSS appears in

the downstream unobstructed region. Compared to the normal aorta, the maximum WSS when δ=40%, δ=60% and δ=80% are increased by 3.6, 8.7, and 34.9 times, respectively. In addition, it is seen that the affecting region of low WSS is also increased.

When the stenosis is unsymmetrical, at the SPA side, the absolute maximum values of WSS are increased to 9.1, 27.7 and 96.1Pa, respectively, when δ=40%, δ=60% and δ=80%. Compared to WSS value when δ=0, it increases by 6.0, 18.4, and 64.3 times, respectively. At SPB side, it increases by 1.7, 4.3, and 11.5 times, respectively. It is seen that with the increase of δ, the position of the maximum WSS moves backward and the influence area becomes larger. Moreover, the alternating low WSS appears in the R4 just as the situation in the symmetrical stenosis.

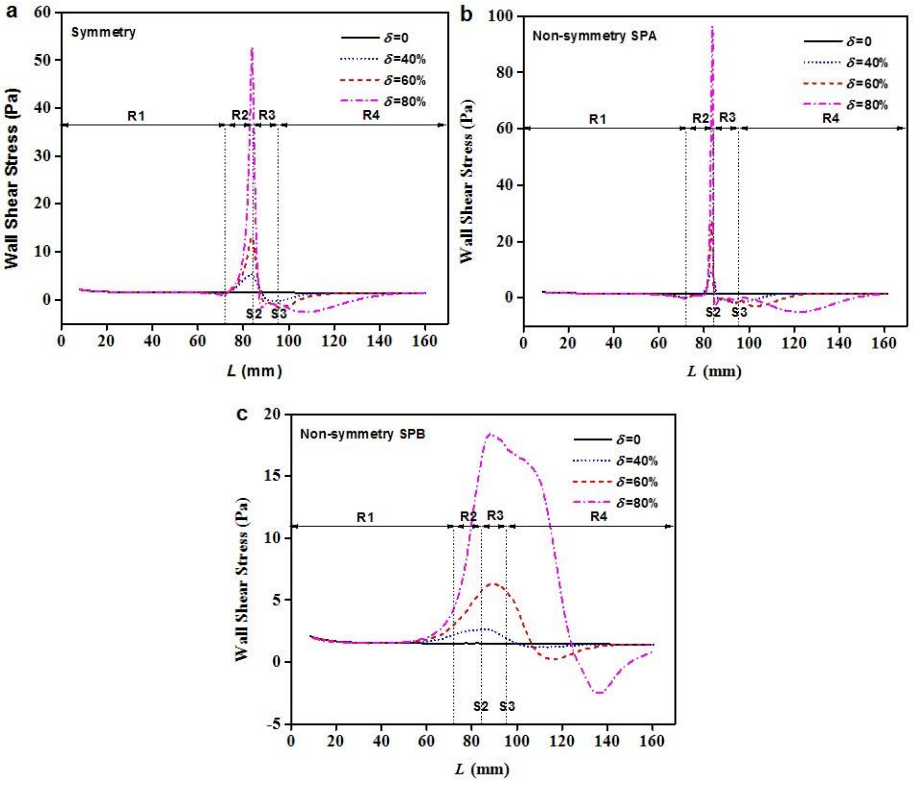

Figure 11: The effect of stenotic ratio on the WSS at t=0.4s: a) symmetrical stenosis; b) unsymmetrical stenosis , SPA side ; c) unsymmetrical stenosis , SPB side.

In order to see clearly the sensitivity of maximum WSS with respect to the stenotic

ratio in symmetrical and unsymmetrical stenosis, Fig. 12 shows the variation of the normalized maximum WSS along with the increase of the stenotic ratio. It is seen that when the stenotic ratio is increased, the normalized maximum WSS is also increased. When the stenotic ratio is larger than a certain value, see, approximately 60% in the present discussion, a little increase of stenotic ratio will cause a dramatic increase of the maximum value of WSS. It is noticed that the maximum WSS at SPA side in unsymmetrical stenosis is larger than that in symmetrical stenosis, but at SPB side, it is lower than that in symmetrical model. At SPA side, WSS displays a higher sensitivity to the variaton of stenotic ratio.

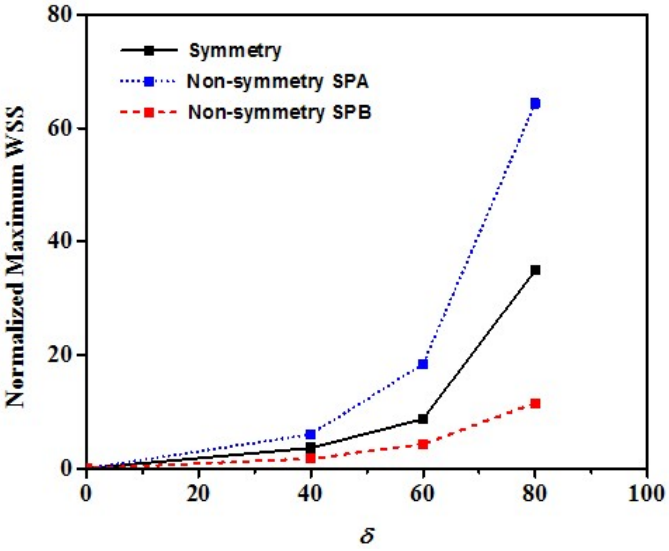

Figure 12: The variation of the normalized maximum WSS with respect to the stenotic ratio for symmetrical or unsymmetrical stenosis.

3.4 Von Mises stresses

If the stress value exceeds the mechanical failure strength of the aortic wall, the intimal damage may occur. In the present discussion, the Von Mises stress is used to measure the effect of the blood flow on the aortic wall stress distribution.

Fig.13 shows the variation of the maximum Von Mises stresses in different layers along the axial direction when δ=0 and δ=40% at t=0.4s. According to Khanafer and Berguer [2], the stress is highest in the media layer and lowest in the intima layer. As shown in Fig.13, the Von Mises stresses in different layers remain unchanged along the axial direction when δ=0 at t=0.4s. For the symmetrical steno-

sis, the Von Mises stress in media layer is a little increased. In R2 and R3 regions, Von Mises stresses in different layers are reduced; whilst they reach the peak value at the throat of the stenosis (at Z= 84mm).

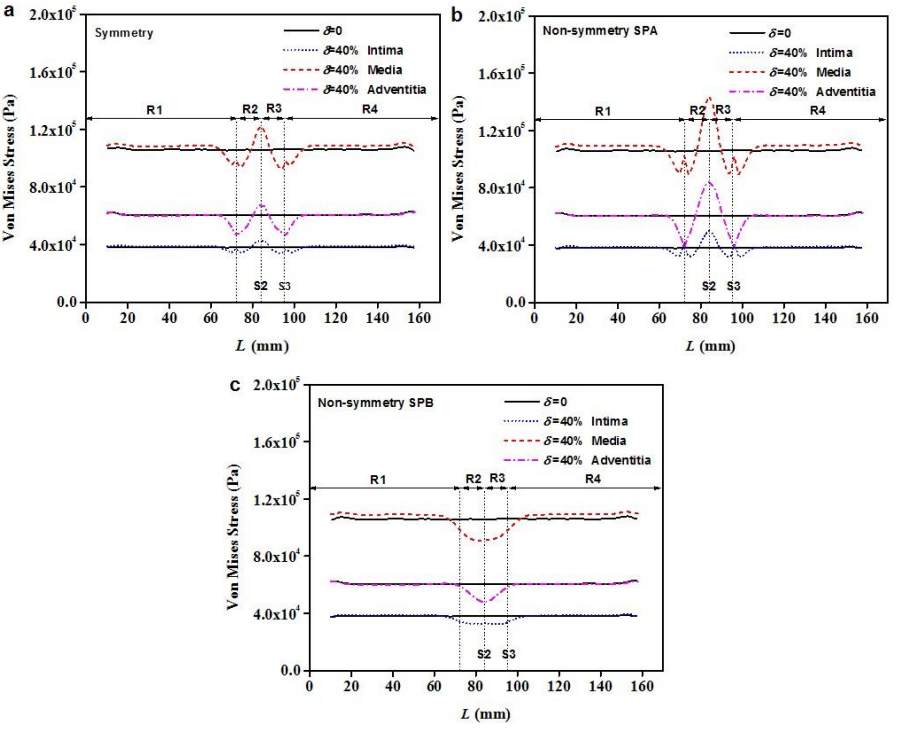

Figure 13: Variation of the maximum Von Mises Stress along the axial direction at t=0.4s.

In the unsymmetrical stenosis, Von Mises stresses in media layer at SPA and SPB sides are both increased. However, at SPA side, it corresponds to more sevious variation of Von Mises stress and higher peak values, especially in the media layer. However, at SPB side, near the throat (in R2 and R3), the Von Mises stresses are decreased compared to that in normal aorta (δ=0). That is, in the aorta with unsymmetrical stenosis, the domain at SPA side near the stenosis is more dangerous considering the dramatic variation of Von Mises stress in media layer.

3.5 Interface shear stress distribution

Interface shear stress is another key parameter which should be given in the description of the aortic dynamic properties. When the stress is greater than the interface shear strength limit, the tearing may occur at the interfaces. In the present discussion, the variation of interface shear stresses along the axial direction when δ=0 and δ=40% at t=0.4s is given in Fig. 14. In the figures, FSI, IMI, and MAI refer to the fluid-solid interface, intima-media interface and media-adventitia interface, respectively.

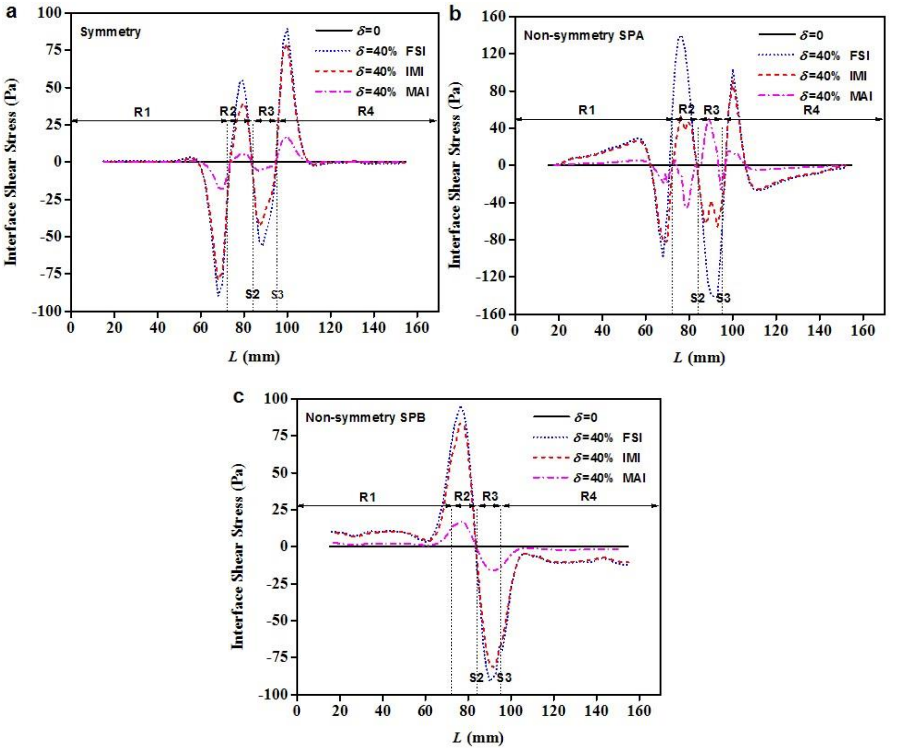

Figure 14: Variation of interface shear stresses along the axial direction at t=0.4s.

For the symmetrical stenosis, it is seen that there is a abrupt stress drop before the throat (Fig. 14a). Then the stresses are increased and then decreased before and after the throat, approximately symmetry about S2. After S3, an abrupt stress up appears with almost the same amplitude as the drop before the stenosis in R1. That is, before and after stenosis, there exist a sharp stress drop and up at the transition cross sections with almost the same amplitude. In the stenosis domain (in R2 and

R3), the interface shear stresses show symmetrical variatoin about S2. The sign of the stresses is changed which indicates the variatoin of the shear direction at the critical cross sections.It is noticed that the stress values at FSI is biggest, and at MAI, the smallest.

For the unsymmetrical stenosis, at SPA side, the basic changing rules of interface shear stresses at FSI and IMI are similar as those in the symmetrical model. But the stresses at FSI and IMI are larger than those in normal aorta and increased from the ends to the stenosis domain. Moreover, it is noticed that the stress at FSI in the stenosis domain is intensively incresased along with the increase of the stenotic ratio. The stress at MAI displays opposite variation rule compared to that at FSI or IMI. At SPB side, the stress distribution shows different characteristics. The stress values are increased due to the existence of the stenosis, especially for stresses at FSI and IMI. It is seen that on the both sides of S2, there form a sharp stress up and drop, which is different from the stress distribution near the stenosis domain in symmetrical stenosis or that on the SPA side of unsymmetrical stenosis. The maximum interface shear stresses appear at the middle of R2 and R3 regions. At S2, shear direction changes.

It is seen that the stress level at fluid-solid interface is higher than that at the intima-media interface, which is greater than that at media-adventitia interface. Moreover, it should be pointed out that the stress sign variation near the stenosis indicates the variation of the shear direction which increases the opportunity of shear damage at the transition plane.

4 Conclusions

In this paper, the coupled dynamic responses of aorta with symmetrical or unsymmetrical stenosis are investigated by using fully coupled fluid-structure interaction analysis based on a three-layered aorta model. From the results above, we can conclude that:

(1) The existence of stenosis causes the variation of the fluid velocity and pressure distributions near the throat (in R2 and R3), and the whirlpool forms at the downstream region (in R4). The non-symmetry of stenosis causes the unsymmetrical distribution of the blood velocity and pressure field in the aorta.

(2) The throat of stenosis is a dangerous plane. WSS and Von Mises stress reach the maximum values at this plane. Moreover, the upstream and downstream fronts of stenosis are also dangerous planes considering the higher absolute interface shear stress values, as well as the variation of the shear directions across the planes.

(3) Along with the increase of the stenotic ratio, the stress in the aorta wall is also increased, and the higher the stenotic ratio, the more sensitivity of this variation

is. The non-symmetry of the stenosis causes the increase of the wall stress and the sensitivity to the stenotic ratio at SPA side compared to those in the aorta with symmetrical stenosis; whist at SPB side, the values are lower than those in aorta with symmetrical stenosis.

These results are helpful for better understand the effects of stenosis on the pathological evolution of cardiovascular diseases.

Acknowledgement: This work is financially supported by National Science Foundation of China (No. 11272046), the National High Technology Research and Development Program of China (863 Program, No. 2013AA030901), and 111 project The first author also would thanks for the support from the Program for New Century Excellent Talents in University (NCET)

References

1. Gao, F., Watanabe, M. & Matsuzawa, T. (2006) Biomed Eng Online 5, 1-11.
2. Khanafer, K. & Berguer, R. (2009) J. Biomech. 42, 2642-2648.
3. Ang, K. C. & Mazumdar, J. N. (1997) Math. Comp. Modelling 25, 19-29.
4. Kagadis, G. C., Skouras, E. D. & Bourantas, G. C. (2008) Med. Eng. Phys. 30, 647-660.
5. Bark Jr, D. L. & Ku, D. N. (2010) J. Biomech. 43, 2970-2977.
6. Melih Guleren, K. (2013) J. Biomech. 46, 1043-1052.
7. Schulze-Bauer, C. A., Morth, C. & Holzapfel, G. A. (2003) J. Biomech. Eng. 125, 395–406.
8. Forrester, J. H. & Young, D. F. (1970) J. Biomech. 3, 297-305.
9. Mills, C. J., Gabe, I. T., Gault, J. H., Mason, D. T., Ross, J., Braunwald, E. & Shillingford, J. P. (1970) Cardiovasc Res. 4, 405-417.
10. Wilcox, D. A. (1994) AIAA J. 32, 247-255.
11. Priymak, V. G. & Miyazaki, T. (1998) J. Comp. Phys. 142, 370-411.
12. Shemer, L., Wygnanski, I. & Kit, E. (1985) J. Fluid Mech. 153, 313-37.
13. Liu, J. S., Lu, P. C. & Chu, S. H. (2000) J. Biomech. Eng. 122, 118-124.
14. Malek, A. M., Alper, S. L. & Izumo, S. (1999) J. Am. Med. Assoc. 282, 2035-2042.